Chen *et al. Biology Direct* (2025) 20:35
https://doi.org/10.1186/s13062-025-00636-9

Biology Direct

RESEARCH Open Access

Prognostic and immunological implications of protein kinases in gastric cancer: a focus on hub gene ABL2 and its impact on the polarization of M2 macrophages

Di Chen[1†], Ju Huang[2†], Aiming Yang[2*] and Zhifan Xiong[3*]

Abstract

Background Protein kinases are essential cellular signal modulators involved in tumorigenesis, metastasis, immune response, and drug resistance. However, the comprehensive features and clinical significance of protein kinases in gastric cancer (GC) remain inconclusive.

Methods We analyzed the transcriptional profiles of protein kinases in GC patients from the GEO and TCGA databases. Based on differentially expressed kinase genes (DE-KGs), a novel cluster was identified to assess its association with patient survival and the tumor microenvironment (TME) in GC. Subsequently, an optimal DE-KGs-based model (DE-KGsM) was determined using 101 machine-learning algorithm combinations. This model was evaluated using multi-omics data to investigate its associations with patient prognosis, clinical features, tumor microenvironment, tumor-infiltrating immune cells (TIICs), and immunotherapy response. Furthermore, scRNA-seq analysis and TIMER algorithm were applied to determine the correlation between the hub gene (ABL2) in the DE-KGsM and Macrophages. Finally, in vitro experiments were performed to explore the immune-related mechanisms of ABL2 in GC.

Results We identified two molecular subtypes of GC patients based on 64 DE-KGs expression. Significant differences were observed in overall survival and TIIC characteristics between Cluster 1 and Cluster 2. Among these 64 DE-KGs, we identified an optimal DE-KGsM that could be a prognostic indicator in GC. TIICs and TIDE analyses exhibited that GC patients in the high-DE-KGsM score group had a higher proportion of M2 macrophages and lower response rates to ICI treatment. scRNA-seq analysis indicated that ABL2 might play an indispensable role in tumor immunity. Furthermore, in vitro experiments demonstrated that ABL2 accelerated the proliferation, migration, and invasion of GC cells, as well as the polarization of M2 macrophages.

[†]Di Chen and Ju Huang contributed equally to this work.

*Correspondence:
Aiming Yang
yangaiming@medmail.com.cn
Zhifan Xiong
1992ly0503@hust.edu.cn

Full list of author information is available at the end of the article

Conclusions The DE-KGsM could be a powerful predictor of GC patients' survival and might facilitate the development of personalized therapy. Furthermore, as a hub gene in the DE-KGsM, ABL2 could be an immunological biomarker that modulates the polarization of M2 macrophages, thereby promoting GC progression.

Clinical trial number Not applicable.

Keywords Protein kinases, scRNA-seq analysis, Gastric cancer, Prognosis, Machine learning, M2 macrophages, ABL2

Introduction

Gastric cancer (GC), a crucial cancer of the gastrointestinal tract, is responsible for more than 1,000,000 new cancer cases and ranked fifth in terms of cancer incidence in 2020 [1]. Despite considerable advancements in diagnostic and therapeutic technologies, the 5-year survival rate for GC patients remains pessimistic. The current standard for predicting the prognosis of GC patients primarily depends on the TNM staging system established by the UICC and AJCC [2]. Nevertheless, patients with the same TNM classification sometimes present different survival outcomes due to the biological heterogeneity and complexity of GC. Hence, it is of great significance to clarify the molecular mechanism of GC initiation and progression, develop promising diagnostic and prognostic biomarkers, and provide individualized treatment strategies.

The tumor microenvironment (TME), a complex and dynamic multicellular ecosystem, functions as a critical regulator in both the initiation and progression of tumors [3]. Recent advancements in scRNA-seq technologies have provided novel insights into the TME [4–6]. Accumulating evidence indicates that the intricate interactions among stromal cells, immune cells, and extracellular mediators play a key role in driving the uncontrolled proliferation, metastatic dissemination, and therapeutic resistance of tumors [7–9]. This biological insight has led to significant breakthroughs in immunotherapy strategies targeting TME components, which brought new hope for tumor patients [10–12]. Tumor immunotherapy enhances the anti-tumor capabilities of immune cells through cellular immunotherapy, immune checkpoint inhibitors, and tumor vaccines, therefore improving therapeutic efficacy [13–15]. With the development of tumor immunotherapy, several options are available for GC. For example, the phase 3 ATTRACTION-2 trial revealed that the survival time of advanced GC patients was shorter in the placebo group than in the nivolumab group (5.3 vs. 4.1 months) [16]. In a phase 1b study, sintilimab plus CapeOx as first-line therapy showed a good response in advanced or metastatic gastric adenocarcinoma (objective response rate: 85.0%) [17]. However, due to the lack of effective therapeutic targets and the heterogeneity of tumor microenvironment (TME), only a small proportion of GC patients benefit from immunotherapy. Therefore, it is of great significance to explore effective immunotherapy targets to enhance the efficacy of cancer immunotherapy.

Protein kinases represent one of the most critical protein families, constituting approximately 2% of the human protein-coding genome [18]. They are essential regulators of signal transduction pathways and control nearly all aspects of cell life, including cell cycle progression, inflammation, metabolism, apoptosis, adhesion, differentiation, and death [19–21]. The disruption of protein kinase functions by dysregulation, altered expression, or mutation can cause cancer and other diseases [22]. Accumulating evidence indicates that protein kinases are significantly associated with tumorigenesis, metastasis, and resistance to chemotherapy in various tumors. For example, the c-Jun N-terminal kinases (JNK), a key category of mitogen-activated protein kinases (MAPK), play tumor suppressor or promoter roles in different tumors. JNK could be activated via growth factors, immune cells, and pro-inflammatory cytokines to promote tumor development [23, 24]. JNK could also regulate the epithelial-mesenchymal transition (EMT) process, thereby influencing tumor metastasis [24, 25]. The Abelson (ABL) family of protein kinases, which includes ABL1 and ABL2, has been found to be upregulated and activated in multiple cancers, indicating a significant correlation between ABL kinase activity and tumor progression [26–30].

Exploring the dysregulation of protein kinases in tumors not only provides valuable insights into oncogenic mechanisms but also contributes to the development of new therapeutic strategies. To date, protein kinases have been discovered to play an indispensable role in the progression of multiple tumors. However, the molecular mechanism of protein kinases has not been elucidated, especially its function in the tumor microenvironment (TME) and tumor immunity. In this study, we analyzed the transcriptional profiles of protein kinases in GC patients. According to the expression of differentially expressed kinase genes (DE-KGs), we identified a novel cluster to assess its association with patient survival and the TME in GC. Then, we established an optimal DE-KGs-based model (DE-KGsM) using 101 combinations of 10 machine-learning algorithms. The DE-KGsM could be a prognostic predictor in GC and associated with tumor-infiltrating immune cells (TIICs). More interestingly, we found that ABL2 within the DE-KGsM is related to the polarization of M2 macrophages. In vitro experiments

further demonstrated that ABL2 could accelerate the proliferation, migration, and invasion of GC cells, as well as the polarization of M2 macrophages.

Materials and methods

Data collection and processing

Figure 1 shows a flowchart of the study. Gene expression and relevant clinical data of GC were extracted from the TCGA and GEO databases (GSE15459 and GSE54129). Single-cell RNA sequencing (scRNA-seq) data of GC was extracted from the GEO databases (GSE112302). The R package "limma" was utilized to identify differentially expressed genes (DEGs) between GC and normal tissues. The cutoff criteria of DEGs were|Log2FC|> 1 and FDR < 0.05. A total of 514 kinase genes (KGs) were obtained from the KinBase database (http://kinase.com/human/kinome) [19]. Overlapping genes between KGs and DEGs were identified as differentially expressed KGs (DE-KGs) for further analysis.

Non-negative matrix factorization (NMF) clustering of DE-KGs

Based on the expression of DE-KGs, NMF clustering was employed to categorize GC patients into distinct clusters. The samples were decomposed into clusters for $k = 2–10$. The common member matrix's average contour width was identified via the "NMF" package in R. According to dispersion, silhouette, and cophenetic, we determined the optimal number of clusters. Kaplan-Meier (KM) analysis was performed to compare the overall survival (OS) in different clusters of GC patients via the R language loaded with packages "survival" and "survminer". Additionally, ESTIMATE and CIBERSORT algorithms and single-sample Gene Set Enrichment Analysis (ssGSEA) were utilized to explore the immune infiltration landscape of TME in different clusters.

Machine learning-based construction of DE-KGsM

To identify potential prognostic DE-KGs, we intersected the above DE-KGs with KGs from GSE15459 and conducted univariate Cox regression analysis using the R package "survival". Subsequently, 101 combinations of 10 machine-learning algorithms (Enet, plsRcox, SuperPC, stepwise Cox, RSF, Ridge, Survival-SVM, GBMs, CoxBoost, and Lasso) were applied to construct a consensus DE-KGsM with high stability and accuracy. The TCGA dataset was set as the training cohort, and the GSE15459 dataset was set as the validation cohort. Harrell's concordance index (C-index) was calculated to assess the performance of 101 algorithm combinations in all cohorts. According to the highest average C-index, we identified the optimal model. DE-KGsM risk scores of GC patients were calculated according to DE-KGs expression and their corresponding coefficients in the optimal model.

Evaluation of DE-KGsM performance

The predictive power and potential clinical applications of the optimal DE-KGsM were evaluated using risk scores of each GC patient. The median DE-KGsM risk score was regarded as the threshold to classify GC patients into the low-DE-KGsM score and high-DE-KGsM score groups. KM analysis was conducted to assess the predictive power of DE-KGsM in the survival outcomes of GC patients. Receiver operating characteristic curves (ROC) were generated using the R package "timeROC" to assess the diagnostic accuracy of DE-KGsM. To improve the clinical applicability of DE-KGsM, a prognostic nomogram was constructed based on the gene signature and clinical features (age, grade, stage, and gender) to predict GC patients' survival quantitatively.

Analysis of immune characteristics and immunotherapy efficacy

To identify the immune characteristics of GC patients, ESTIMATE and CIBERSORT algorithms were applied to calculate the composition of different tumor-infiltrating immune cells (TIICs) based on the transcriptome data. To evaluate the disparities in immune function status between low and high-DE-KGsM score groups, ssGSEA was carried out using the "GSVA" package in R software. Then, the difference analysis was performed to clarify the heterogeneity of TIICs between the high-DE-KGsM and low-DE-KGsM score groups. Correlation analyses were carried out to identify TIICs associated with DE-KGsM risk scores. Based on the difference and correlation analyses, we identified the crucial immune cells (M2 macrophages) for further investigation. Furthermore, the Tumor Immune Dysfunction and Exclusion (TIDE) algorithm was applied to assess differences in immunotherapy efficacy between GC patients with low vs. high DE-KGsM scores.

ScRNA-seq, immunological, differentially expressed, and prognostic analyses

To investigate the cellular distribution of DE-KGs in the model, we downloaded scRNA-seq data of GC samples from the GEO database (GSE112302 and GSE167297). Specifically, GSE112302 comprises 6 GC samples, while GSE167297 includes 10 GC samples. UMAP algorithm was utilized to identify and visualize cell clusters. Cell clusters were further assigned by combining Cell Typist and the 'singleR' function. Subsequently, DE-KGs in the model co-distributed with macrophages were identified as hub DE-KGs (ABL2) via scRNA-seq analysis. To further confirm the results of scRNA-seq analysis, MCPCOUNTER, CIBERSORT-ABS, TIMER, and QUANTISEQ algorithms were utilized to analyze the correlation between the expression level of ABL2 and Macrophages. Scatter plots were used to visualize the

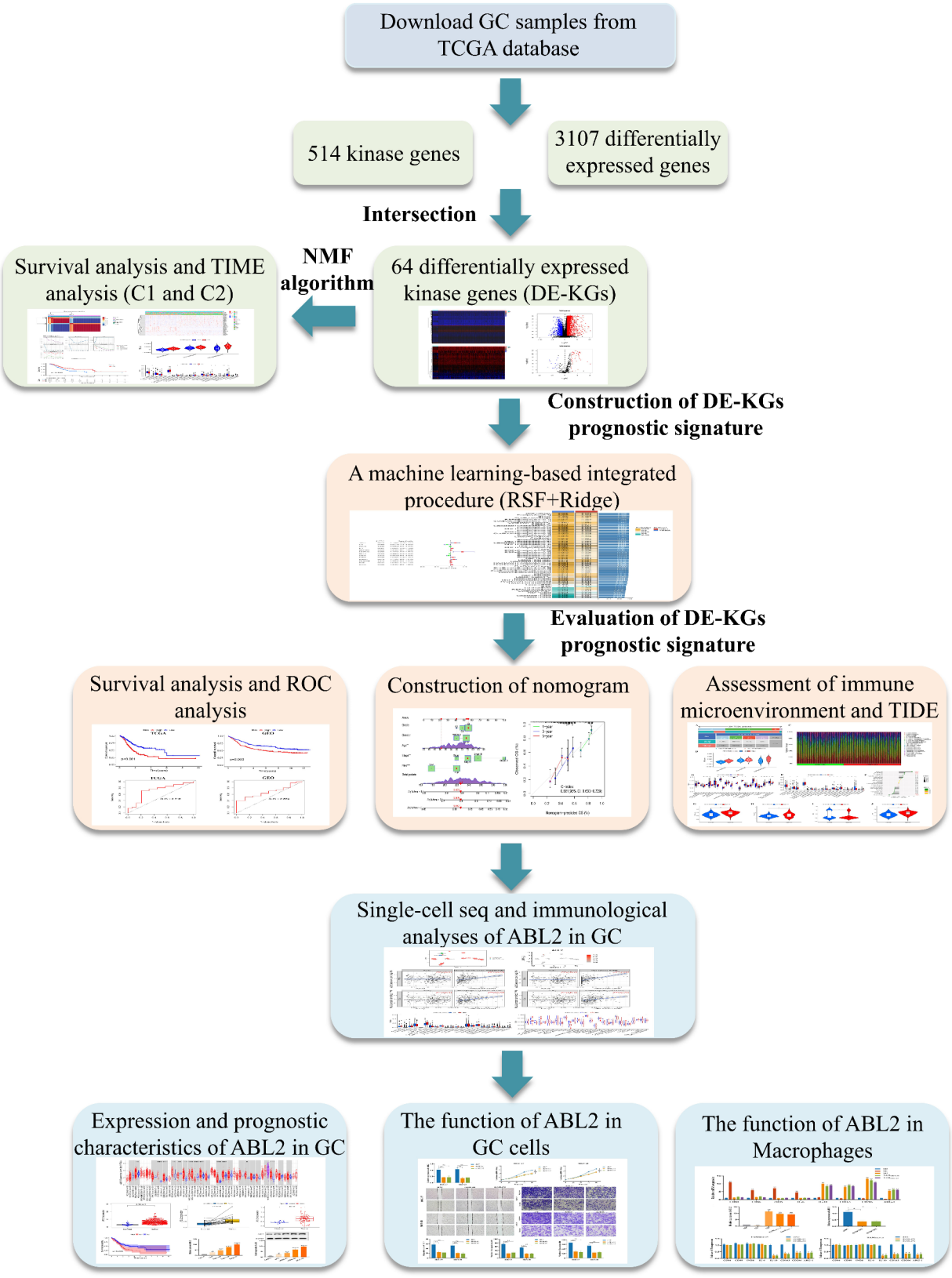

Fig. 1 Flowchart of the study

positive correlation between ABL2 expression and M2 macrophages. To further investigate the immune-related role of ABL2 in GC, the R package "limma" was utilized to classify 339 GC cases into ABL2-low and ABL2-high groups. Then, ssGSEA was performed to explore the differences in immune-related functions and TIICs between ABL2-low and ABL2-high groups via the R packages "GSEABase" and "GSVA". Furthermore, ABL2 expression differences between tumor and normal samples were identified in pan-cancers based on TIMER2 (https://timer.cistrome.org/) online databases. We also downloaded the GSE54129 dataset from the GEO to validate ABL2 expression at the mRNA levels in GC.

Cell culture and macrophage differentiation

THP-1 and GC cells (MKN-28, HGC-27, and MKN-45) were cultured in RPMI-1640 (Gibco, USA) containing 10% or 20% fetal bovine serum (FBS) (Gibco, USA). GC cells (AGS) and gastric mucosal cells (GES-1) were cultured in F-12 K (Gibco, USA) supplemented with 10% FBS or DMEM (Gibco, USA) supplemented with 10% FBS, respectively. Two shRNAs for ABL2 (sh-ABL2#1 and sh-ABL2#2) and a negative control (sh-NC) were synthesized by Gikai gene (Shanghai, China). According to the manufacturer's protocol, they were transfected using lentivirus vectors. To differentiate into M0 macrophages, THP-1 cells were treated with 100ng/ml PMA (Sigma, USA) for 48 h. For the induction of M1 macrophages, M0 macrophages were treated with 20ng/ml IFN-γ(MCE, USA) and 100ng/ml LPS (MCE, USA) for 48 h. For the induction of M2 macrophages, M0 macrophages were treated with 20ng/ml IL-4 (MCE, USA) and 20ng/ml IL-13 (MCE, USA) for 48 h. For the induction of TAMs(TAM_{MKN-28}, and TAM_{HGC-27}), M0 macrophages were co-cultured with GC cells (MKN-28 and HGC-27) for 48 h.

Table 1 The sequence of primers

Primer	Forward (5'-3')	Reverse (5'-3')
ABL2	GTTGAACCCCAGGCACTAAAT	CAACGAAGAGATTAGGGTCACTC
Arg-1	GTGGAAACTTGCATGGACAAC	AATCCTGGCACATCGGGAATC
IL-6	ACTCACCTCTTCAGAACGAATTG	CCATCTTTGGAAGGTTCAGGTTG
IL-10	GACTTTAAGGGTTACCTGGGTTG	TCACATGCGCCTTGATGTCTG
iNOS	ACCTTGTTCAGCTACGCCTT	CATTCCCAAATGTGCTTGTC
CD163	TTTGTCAACTTGAGTCCCTTCAC	TCCCGCTACACTTGTTTTCAC
CD206	TCCGGGTGCTGTTCTCCTA	CCAGTCTGTTTTTGATGGCACT
CD80	AAACTCGCATCTACTGGCAAA	GGTTCTTGTACTCGGGCCATA
CD86	TATGGGCCGCACAAGTTTT	TGGTGGATGCGAATCATTCCT
GAPDH	CTCGCTTCGGCAGCACA	AACGCTTCACGAATTTGCGT

Quantitative real-time polymerase chain reaction (qRT-PCR) and Western blotting (WB)

RNA-easy Isolation (Vazyme, Nanjing, China) was used to extract Total RNAs from cell lines. cDNA was synthesized using HiScript II 1st Strand cDNA Synthesis Kit (Vazyme, Nanjing, China). After reverse transcription, Green Master Mix (Vazyme, Nanjing, China) was used to conduct qRT-PCR. Primer sequences are listed in Table 1. Total protein was extracted using RIPA Lysis Buffer, separated by SDS-PAGE, and transferred to PVDF membranes. Then, membranes were incubated overnight with the primary antibody against ABL2 (Abcam, UK) and GAPDH (Proteintech, Wuhan, China). Finally, membranes were incubated with secondary antibodies and visualized by the ECL detection system.

CCK-8, wound healing, and transwell assays

The proliferation ability of GC cells was determined by CCK-8 assay according to the manufacturer's protocol. Transfected GC cells (4×10^3/well) were plated in 96-well plates and incubated for 24, 48, and 72 h. Then, each well was added with 10 μL CCK-8 (Vazyme, Nanjing, China), and absorbance (450 nm) was measured using a microplate reader. Cell migration potential was measured using wound healing and Transwell migration assays. GC cells were cultured to 90% confluence in 6-well plates and scratched straightly using a 200μL pipette tip. The medium was replaced with RPMI-1640, and the position of scratches was photographed at 0 h and 24 h. For Transwell migration assays, GC cells were transferred to the Transwell inserts (Corning, USA) in 100μL RPMI-1640 medium, with 750 μL RPMI-1640 containing 10% FBS added to the lower chamber. After 24 h, cells on the bottom of the membrane were stained with 1% crystal purple and counted under a microscope. To evaluate cell invasion potential, the inserts with precoated Matrigel (BD Biosciences, USA) were utilized to carry out Transwell assays.

Statistical analysis

Data organization, analysis, and graphing were conducted using GraphPad Prism 7.0, R software (version 4.3.1), and Image-pro Plus 6.0. $P < 0.05$ or P-adjusted < 0.05 was defined as statistically significant.

Results

DE-KGs-based clusters and TME analysis

A total of 3107 DEGs were identified between GC and normal tissues, including 2239 upregulated genes and 868 downregulated genes ($|Log2FC| > 1$ and $FDR < 0.05$) (Fig. 2A, B). Among them, 64 DEGs were identified as DE-KGs via intersecting with the 514 kg obtained from the KinBase database (Fig. 2C, D and Table. S1). Based on the expression profiles of these 64 DE-KGs, 339 GC

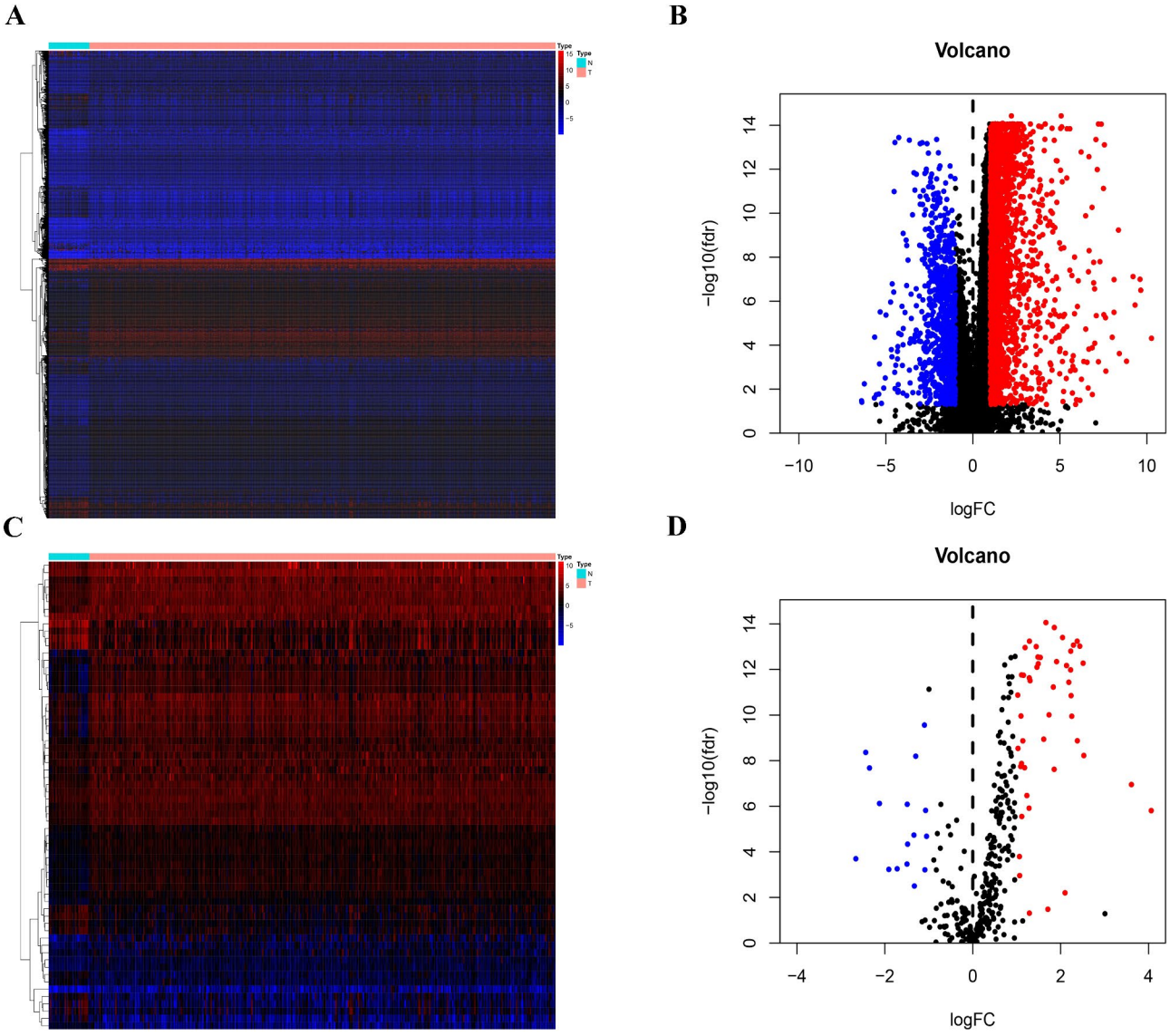

Fig. 2 Analysis of Differentially Expressed Kinase Genes. **(A)** Heatmap of differentially expressed genes in GC. **(B)** Volcano plot of differentially expressed genes in GC. **(C)** Heatmap of differentially expressed kinase genes in GC. **(D)** Volcano plot of differentially expressed kinase genes in GC

patients were classified into two clusters: Cluster 1 ($n = 165$) and Cluster 2 ($n = 174$) (Fig. 3A, B). We analyzed the differences in OS and clinicopathological characteristics between the two clusters. The results revealed that patients in Cluster 1 had a worse prognosis ($P = 0.003$), higher tumor grade ($P < 0.01$), and more advanced T stage ($P < 0.05$) than those in Cluster 2 (Fig. 3C, D). Additionally, we evaluated the differences in the TME between the two clusters. The StromalScore, ImmuneScore, and ESTIMATEScore were significantly elevated in Cluster 1 compared to Cluster 2 ($P < 0.05$) (Fig. 3E). Using the CIBERSORT algorithm, we analyzed the fraction of infiltrating immune cells in different clusters. As shown in Fig. 3F, the proportions of M2 macrophages, Dendritic cells resting, B cells memory, Mast cells activated, T cells follicular helper, and Mast cells resting were remarkably different between Cluster 1 and Cluster 2 ($P < 0.05$). These results indicated that two distinct GC patterns differentiated according to 64 DE-KGs expression, suggesting that survival differences under these DE-KGs may be correlated with immune cell infiltration in the TME.

Construction and evaluation of DE-KGsM

To further elucidate the prognostic value of these DE-KGs, univariate Cox regression analysis was performed to determine DE-KGs associated with the GC patients' survival (Fig. 4A). A machine learning-based integrated procedure was employed to construct a consensus DE-KGsM. Notably, the optimal DE-KGsM was constructed through the algorithm pattern (RSF + Ridge),

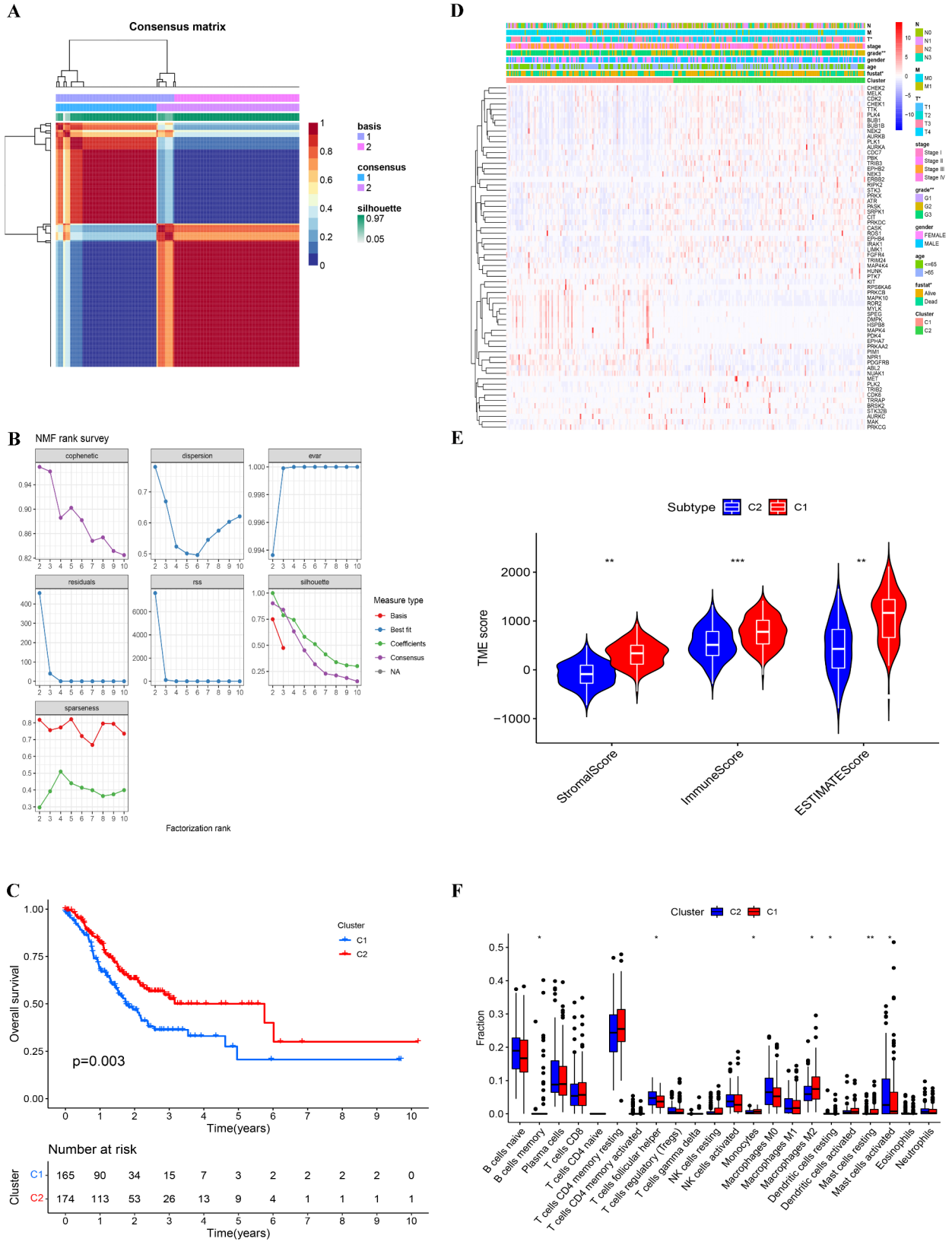

Fig. 3 Identification and characterization of DE-KG-Based clusters. **(A)** Heatmap of sample clustering. **(B)** The distribution of cophenetic, rss, and silhouette with k valued 2 to 10. **(C)** The survival analysis of GC patients in Cluster1 and Cluster2. **(D)** The differences of clinicopathological features between 2 clusters. **(E)** The differences of StromalScore, EstimateScore, and ImmuneScore between 2 clusters. **(F)** The component differences of TIICs between 2 clusters. *$P < 0.05$, **$P < 0.01$, ***$P < 0.001$

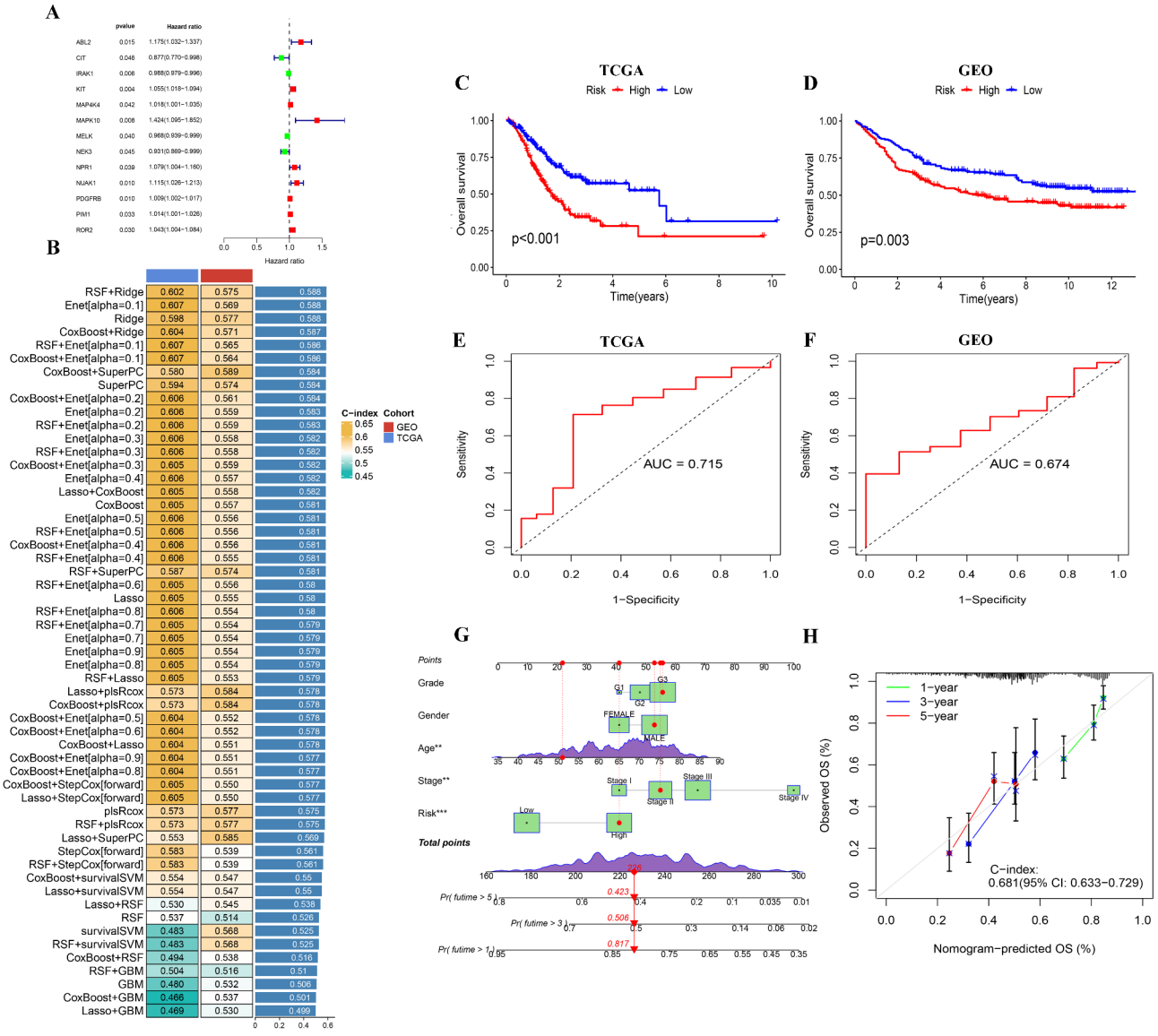

Fig. 4 Construction and evaluation of the DE-KGs-based model in GC. **(A)** Identification of DE-KGs associated with the GC patients' survival. **(B)** Construction of optimal DE-KGs-based model. **(C)** The survival analysis of the DE-KGs-based model in the TCGA. **(D)** The survival analysis of the DE-KGs-based model in the GSE15459. **(E)** ROC analysis of the DE-KGs-based model in the TCGA. **(F)** ROC analysis of the DE-KGs-based model in the GSE15459. **(G)** The construction of nomogram in the TCGA. **(H)** Calibration curves of the nomogram

which achieved the highest C-index (0.602) (Fig. 4B). Then, we identified a total of 13 genes (MAP4K4, PIM1, KIT, IRAK1, ROR2, MAPK10, MELK, NUAK1, CIT, NEK3, ABL2, NPR1, PDGFRB) were identified in the model, and DE-KGsM risk scores were calculated for each sample. According to the median risk score, GC samples were separated into low-and high-DE-KGsM score groups to assess the predictive power and diagnostic accuracy of the optimal DE-KGsM. The KM survival curve depicted that GC patients with a high-DE-KGsM score had significantly lower OS than those with a low-DE-KGsM score in the TCGA ($P < 0.001$), and GSE15459 ($P = 0.003$) cohorts (Fig. 4C, D). KM analysis confirmed the significant predictive power of DE-KGsM in evaluating the prognosis of GC patients. ROC curves indicated high diagnostic efficacy of DE-KGsM at five years in the TCGA (0.715), and GSE15459 cohorts (0.674) (Fig. 4E, F). To improve survival prediction for GC patients, we further established a nomogram based on the prognostic characteristics of DE-KGs and several clinicopathological factors, including grade, stage, gender, and age (Fig. 4G). The calibration plot demonstrated accurate nomogram-predicted OS probabilities for the 1-, 3-, and 5-year survival rates (Fig. 4H).

Identification of specific immune-related mechanisms underlying DE-KGsM

Subsequent investigations elucidated the specific immune-related mechanisms through which DE-KGsM influences the prognosis of GC patients. We evaluated the differences in immune subtype and TME between the two risk groups. As shown in Fig. 5A, C3 (inflammatory subtype) was significantly different between the low- and high-DE-KGsM score groups ($P = 0.001$). As shown in Fig. 5B, GC patients with high-DE-KGsM scores had higher StromalScore, ImmuneScore, and ESTIMATEScore than those with low-DE-KGsM scores ($P < 0.05$). To further explore the association between the DE-KGsM and immune microenvironment, we applied CIBERSORT algorithm to calculate the composition of 22 types of TIICs in GC samples (Fig. 5C). Then, we compared the component differences of immune-related functions and TIICs between the two risk groups. As shown in Fig. 5D, the high-DE-KGsM score group was positively associated with multiple immune-related functions, including Macrophages, B_cells, Parainflammation, Mast_cells, Type_II_IFN_Reponse, CD8+_T_cells, and so on ($P < 0.05$). As shown in Fig. 5E, the high-DE-KGsM score group had higher proportions of M2 macrophages, Mast cells resting, T cells CD8, Monocytes, and Dendritic cells activated ($P < 0.05$). In contrast, the number of Macrophages M1, T cells follicular helper, and Mast cells activated was increased in the low-DE-KGsM score group ($P < 0.05$). Correlation analysis also showed that DE-KGsM risk scores were positively associated with M2 macrophages, B cells naïve, and NK cells resting ($P < 0.05$) (Fig. 5F). Based on the results of differential and correlation

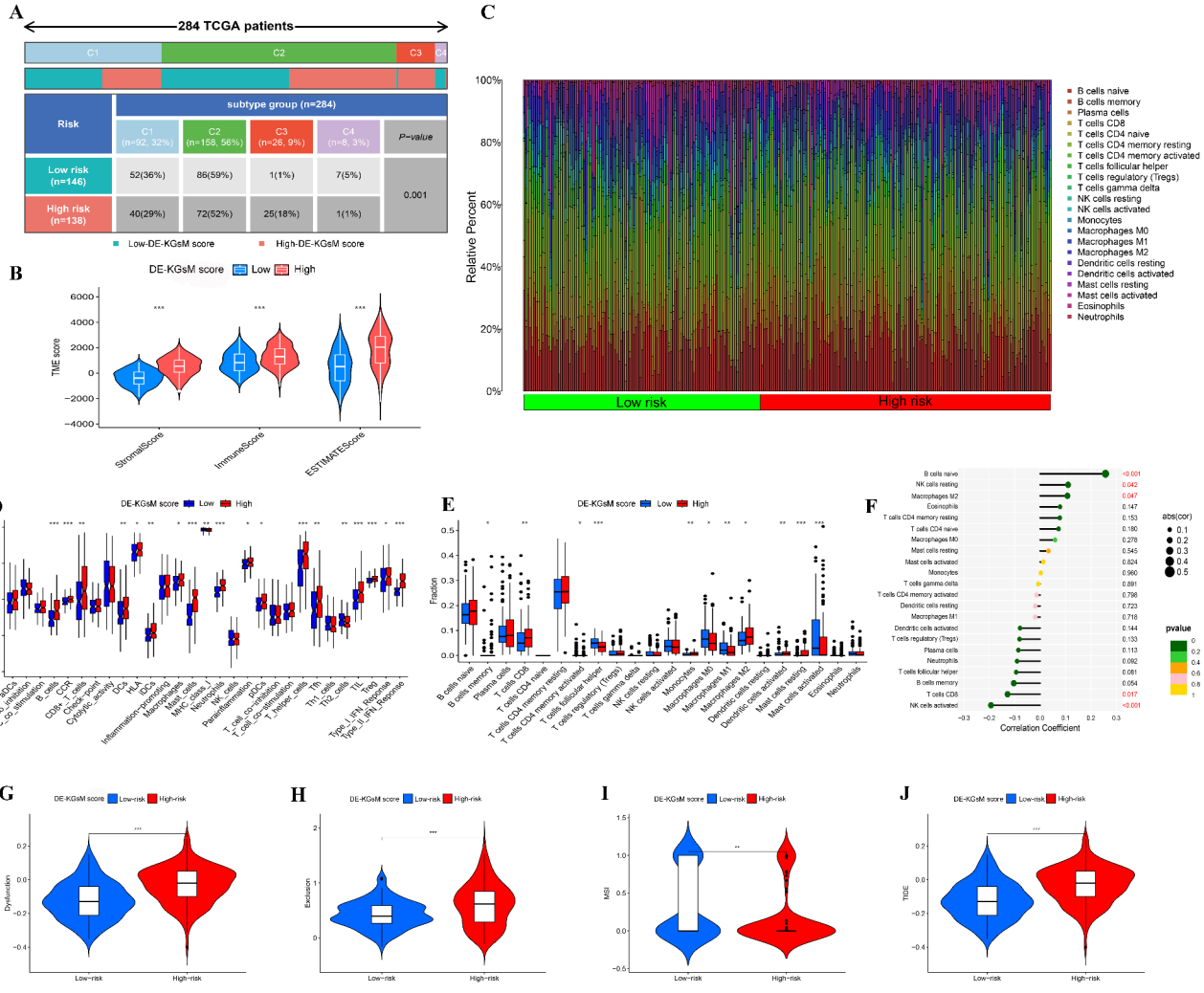

Fig. 5 Comparison of immune microenvironment between high- and low-DE-KGsM score GC patients. **(A)** The differences of immune subtype between high- and low-DE-KGsM score groups. **(B)** The composition of 22 types of TIICs in GC samples. **(C)** The differences of TME between high- and low-DE-KGsM score groups. **(D)** The component differences of TIICs between high- and low-DE-KGsM score groups. **(E)** The differences of 29 immune-related signatures between high- and low-DE-KGsM score groups. **(F)** The correlation analysis of TIICs and risk scores. **(G-J)** The immunotherapy response differences between high- and low-DE-KGsM score GC patients. $^{*}P < 0.05$, $^{**}P < 0.01$, $^{***}P < 0.001$

analyses, we revealed that only the proportion of M2 macrophages exhibited both a significant correlation and a consistent trend with the DE-KGsM risk scores. Furthermore, TIDE analysis revealed that the TIDE score of GC patients in the low-DE-KGsM score group was significantly lower than that in the high-DE-KGsM score group ($P<0.05$) (Fig. 5G-J). These results indicated that elevated DE-KGsM scores are characterized by immune cell infiltration and exert functional influences, particularly in M2 macrophages.

ABL2 immunological implications, expression levels, and prognostic characteristics in GC

Based on the results of component differences in TIICs across different clusters and risk groups, we speculated that hub genes in the DE-KGsM might participate in regulating the function of M2 macrophages in TME. scRNA-seq analysis of GSE112302 and GSE167297 revealed 3 and 10 cell clusters, respectively annotated by UMAP algorithm (Fig. 6A). Among DE-KGs in the model, only ABL2 was co-distributed with Macrophages in both GSE112302 and GSE167297 datasets (Fig. 6B and S1). Therefore, ABL2 was identified as hub DE-KGs for further analysis. Subsequently, MCPCOUNTER, CIBERSORT-ABS, TIMER, and QUANTISEQ algorithms were utilized to further identify the correlation between the expression levels of ABL2 and Macrophages. The correlation analysis indicated that ABL2 expression was positively correlated with tumor infiltration level of M2 macrophages ($P<0.05$) (Fig. 6C). Differences in immune-related functions and TIICs between ABL2-low and high groups were further analyzed using ssGSEA. As shown in Fig. 6D and E, immune-related functions, such as Type II IFN Reponse, Treg, and Macrophages were significantly activated in the ABL2-high group ($P<0.05$). The proportion of TIICs, including M2 macrophages and T cells CD4 memory resting was significantly higher in the ABL2-high group compared to the ABL2-low group ($P<0.05$). We speculated that the hub gene (ABL2) in the DE-KGsM may play an indispensable role in tumor immunity through regulating the status of Macrophages. Therefore, we further investigated the biological functions of ABL2. The differential expression of ABL2 between normal and GC samples was analyzed based on the TCGA database. The increased expression of ABL2 was observed in GC compared to normal samples ($P<0.05$) (Fig. 7A-C). Meanwhile, the expression result of ABL2 in the GSE54129 dataset was consistent with the TCGA database ($P<0.05$) (Fig. 7D). To investigate the prognostic value of ABL2, GC patients from the TCGA database were classified into ABL2-low and ABL2-high groups. The KM survival curves indicated that GC patients with higher levels of ABL2 had a worse OS rate ($P<0.05$) (Fig. 7E).

The expression and function of ABL2 in GC cells and macrophages

Furthermore, qRT-PCR and WB assays were performed to validate the expression of ABL2. ABL2 differential expression levels between normal gastric cells (GES-1) and GC cells (MKN-45, HGC-27, AGS, and MKN-28) were compared using qRT-PCR and WB. The results indicated that the expression of ABL2 was maximally upregulated in HGC-27 and MKN-28 ($P<0.05$) (Fig. 7F, G), further demonstrating that ABL2 was significantly elevated in GC. To evaluate the carcinogenic effect of ABL2 in GC, ABL2 was successfully knocked down in MKN-28 and HGC-27. qRT-PCR results verified substantial transfection efficiency of shABL2#1 and shABL2#2 ($P<0.05$) (Fig. 8A). Subsequently, CCK-8 assay revealed that the proliferation of GC cells was dramatically decreased in shABL2#1 and shABL2#2 groups ($P<0.05$) (Fig. 8B). Wound healing assay proved that silencing ABL2 was sufficient to suppress GC cells migration ($P<0.05$) (Fig. 8C). Transwell migration and invasion assays proved that the knockdown of ABL2 was sufficient to suppress GC cells migration and invasion ($P<0.05$) (Fig. 8D).

To further investigate the potential impact of ABL2 on modulating the function of macrophages, we constructed M0, M1, M2, TAM_{MKN-28}, and TAM_{HGC-27} in vitro. qRT-PCR results indicated that M2 markers (CD206, CD163, Arginase-1 and IL-10) levels were upregulated in TAM_{MKN-28} and TAM_{HGC-27}, while M1 markers (CD80, CD86, iNOS and IL-6) levels were downregulated in TAM_{MKN-28} and TAM_{HGC-27} ($P<0.05$) (Fig. 9A). The above results indicated that TAMs were more likely to express the characteristics of M2 macrophages. Then, qRT-PCR was performed to identify the expression of ABL2 in different types of macrophages. qRT-PCR results showed that ABL2 expression was relatively increased in M2, $TAM_{MKN-28,}$ and TAM_{HGC-27} ($P<0.05$) (Fig. 9B). Furthermore, to investigate the role of ABL2 in macrophages, we carried out loss of function assays. The result of qRT-PCR verified that the transfection efficiency of shABL2#1 and shABL2#2 was substantial ($P<0.05$) (Fig. 9C). qPCR results also demonstrated that M2 markers (CD206, CD163, Arginase-1 and IL-10) levels were significantly downregulated after silencing ABL2 in TAM_{MKN-28} and TAM_{HGC-27} ($P<0.05$) (Fig. 9D, E). These results indicated that ABL2 was indispensable for the generation of TAMs with M2 phenotype. In summary, in vitro experiments revealed that ABL2 accelerated the malignant process of GC via modulating the proliferation, migration, and invasion of tumor cells, as well as the polarization of M2 macrophages, therefore leading to poor prognosis in GC patients.

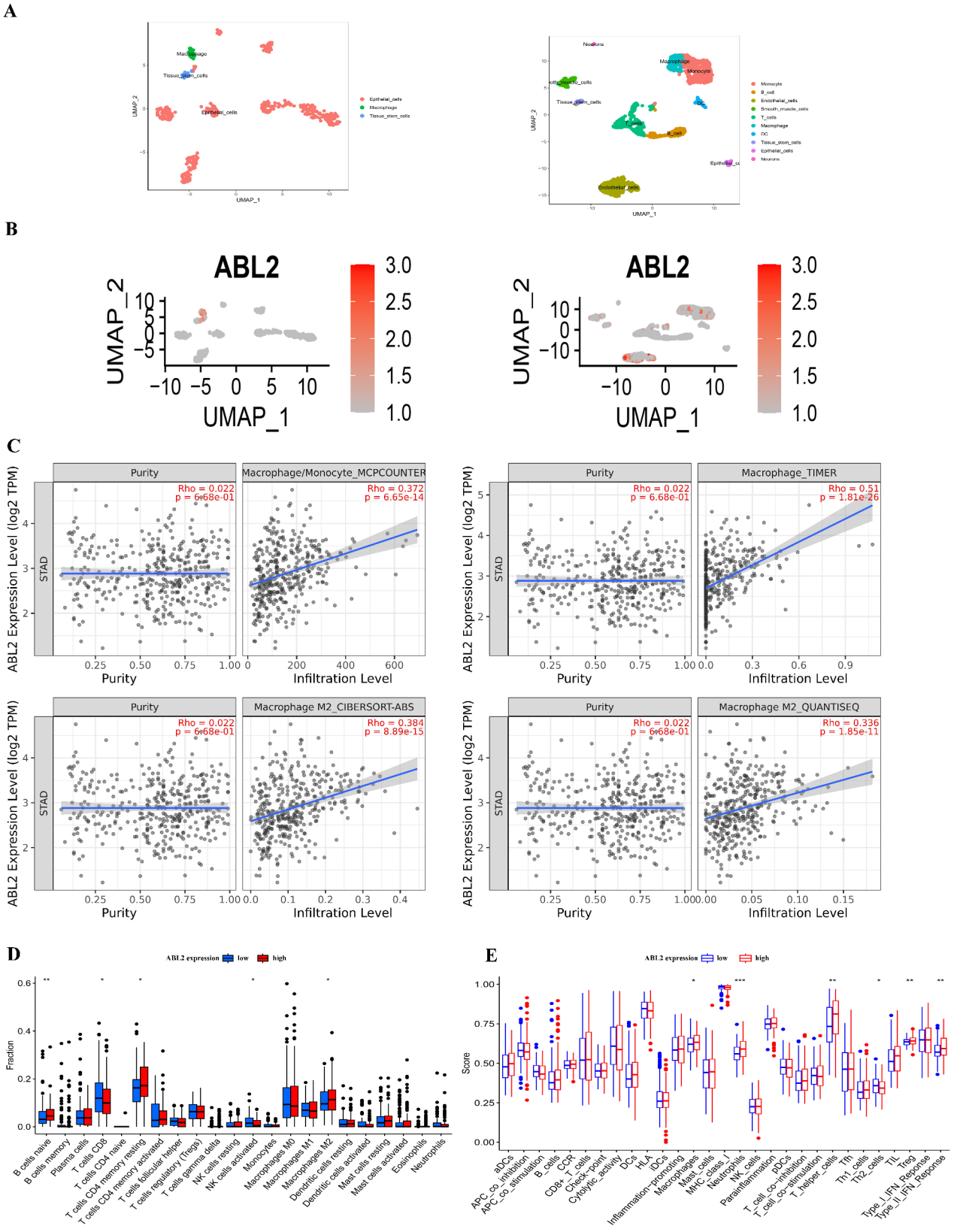

Fig. 6 The association between expression level of ABL2 and Macrophages. **(A)** Cell clustering of scRNA-seq data. **(B)** Distribution of ABL2 in different cell populations. **(C)** The correlation of Macrophages and M2 macrophages proportion with ABL2 expression. **(D)** The component differences of TIICs between the ABL2-high and ABL2-low groups. **(E)** The differences of 29 immune-related signatures between the ABL2-high and ABL2-low groups

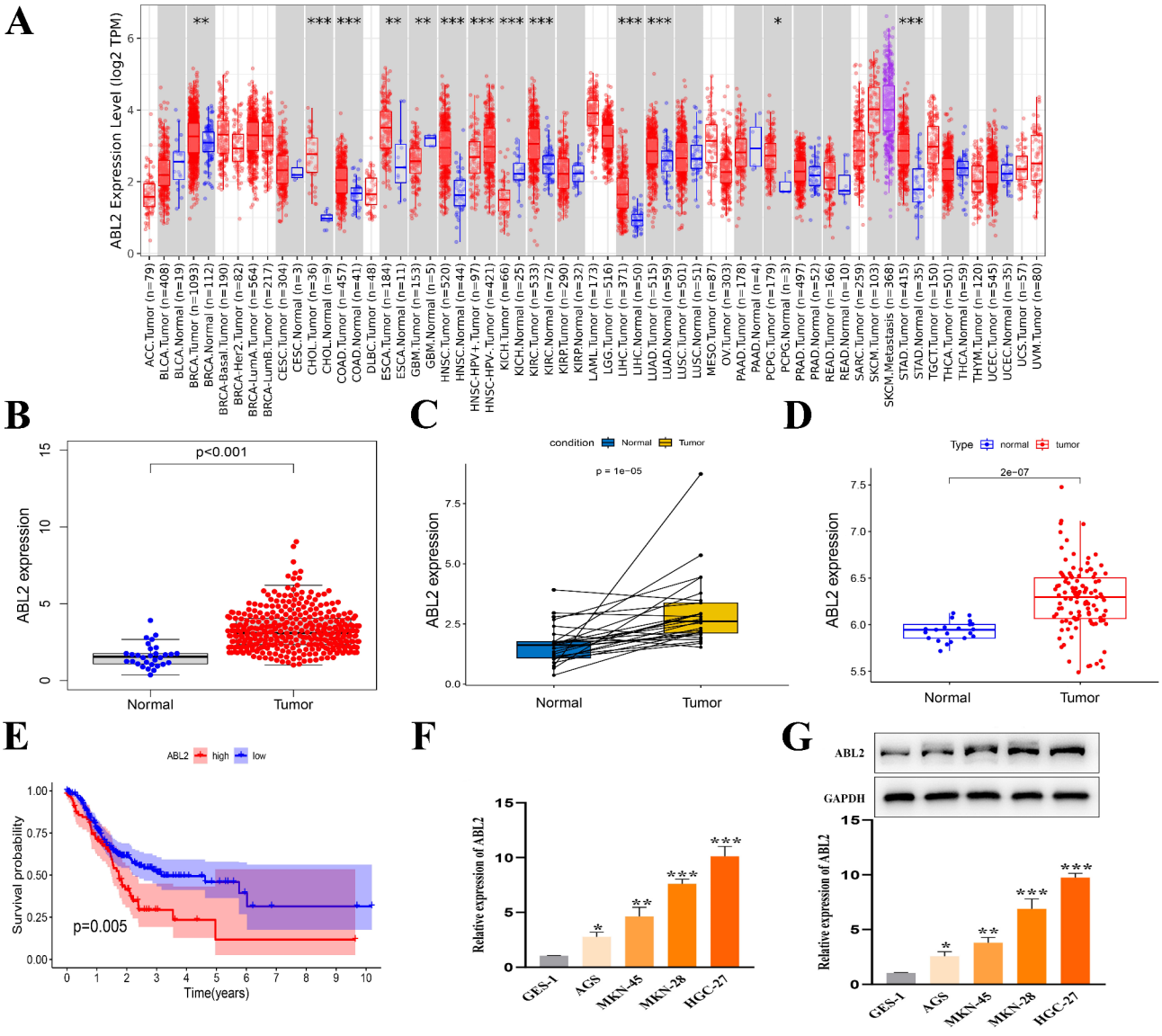

Fig. 7 The expression levels and prognostic characteristics of ABL2 in GC. **(A)** ABL2 expression in tumor and normal samples from the TIMER database. **(B)** ABL2 expression in GC and normal samples from the TCGA database. **(C)** ABL2 expression in the paired GC and normal samples from the TCGA database. **(D)** ABL2 expression in GC and normal samples from the GEO database. **(E)** The survival analysis of GC patients based on ABL2 expression. **(F)** The mRNA expression of ABL2 in GC cells. **(G)** The protein expression of ABL2 in GC cells

Discussion

Protein kinases are critical regulators of cellular signaling and play a pivotal role in modulating various biological processes, including cell migration, proliferation, metabolism, survival, and so on [31]. Over the past decades, advancements in the technology of genomics, proteomics, and bioinformatics have provided novel insights into the dysregulation of the human kinome in tumors [32, 33]. Accumulating evidence indicates that protein kinases are significantly involved in GC progression and prognosis. Therefore, protein kinases may serve as important predictors of clinical outcomes for GC patients. Several studies have revealed that the deregulation of protein kinases is significantly correlated with immune responses in GC progression. For example, Guo et al. found that death-associated protein kinase 1 (DAPK1), a member of the DAPK family of serine/threonine kinases, is involved in the development of GC. The overexpression of DAPK1 facilitates the killing ability of NK cells and suppresses the immune evasion of GC cells [34]. Hsu et al. discovered that serine/threonine-protein kinase 24 (STK24) plays an immunosuppressive role in the tumorigenesis of GC. Mechanistically, the knockdown of STK24 induces $F4/80^+$ macrophages and $CD11b^+$ $Ly6C^+$ MDSCs expansion in orthotopic immunocompetent GC animal models [35]. By using the TCGA database, Wu et al. found that

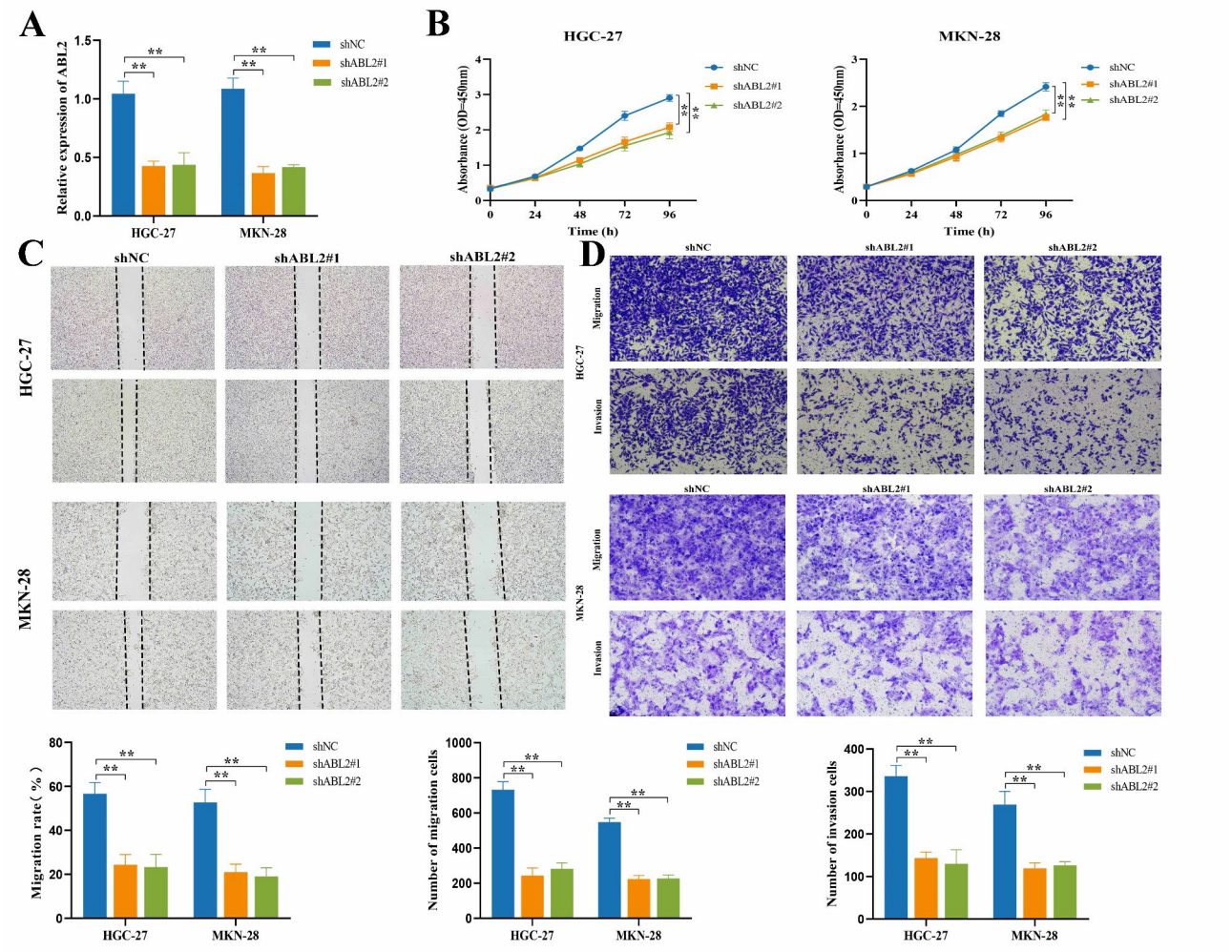

Fig. 8 Effect of ABL2 on the proliferation, migration, and invasion of GC. **(A)** The validation of ABL2 knockdown in HGC-27 and MKN-28. (B) CCK-8 assays were performed to evaluate the effect of ABL2 on GC cell proliferation ability. **(C)** Wound healing assays were performed to evaluate the effect of ABL2 on GC cell migration ability. **(D)** Transwell migration and invasion assays were performed to evaluate the effect of ABL2 on GC cell migration and invasion ability

highly expressed doublecortin-like kinase 1 (DCLK1) is associated with increased immune components in the TME and can predict the worse survival of GC patients. Further analysis suggested that DCLK1 may promote immunotherapy sensitivity in GC via modulating TAM-mediated inhibition of $CD8^+$ T cells [36]. However, few studies have comprehensively explored the survival outcome and immune infiltration characteristics of several KGs combined effects.

In this study, we identified two molecular subtypes of GC patients according to 64 DE-KGs expression. Patients in Cluster 1 had higher tumor grade, more advanced T stage, and worse OS than those in Cluster 2. The characteristics of the TME and infiltrating immune cells were also analyzed in the two clusters. We discovered that higher levels of B cells memory, M2 macrophages, and Mast cells resting were presented in Cluster 1 compared with Cluster 2. Given that Cluster 1 was positively correlated with tumor progression and prognosis, these findings implied that B cells memory, M2 macrophages, and Mast cells resting infiltrated in the GC microenvironment may portend a worse survival. Therefore, we speculated that survival differences under 64 DE-KGs expression might be correlated with immune cells infiltrated in the TME. To improve the accuracy of predicting GC patients' survival, univariate Cox and 101 combinations of machine-learning algorithms were carried out to further construct a 13 DE-KGsM. The survival analysis, ROC curve analysis, and nomogram construction further confirmed that the model could reliably predict the prognosis of GC patients.

TME is increasingly recognized as an indispensable regulator in the initiation, progression, and metastasis of tumors [3]. TIICs, such as macrophages and

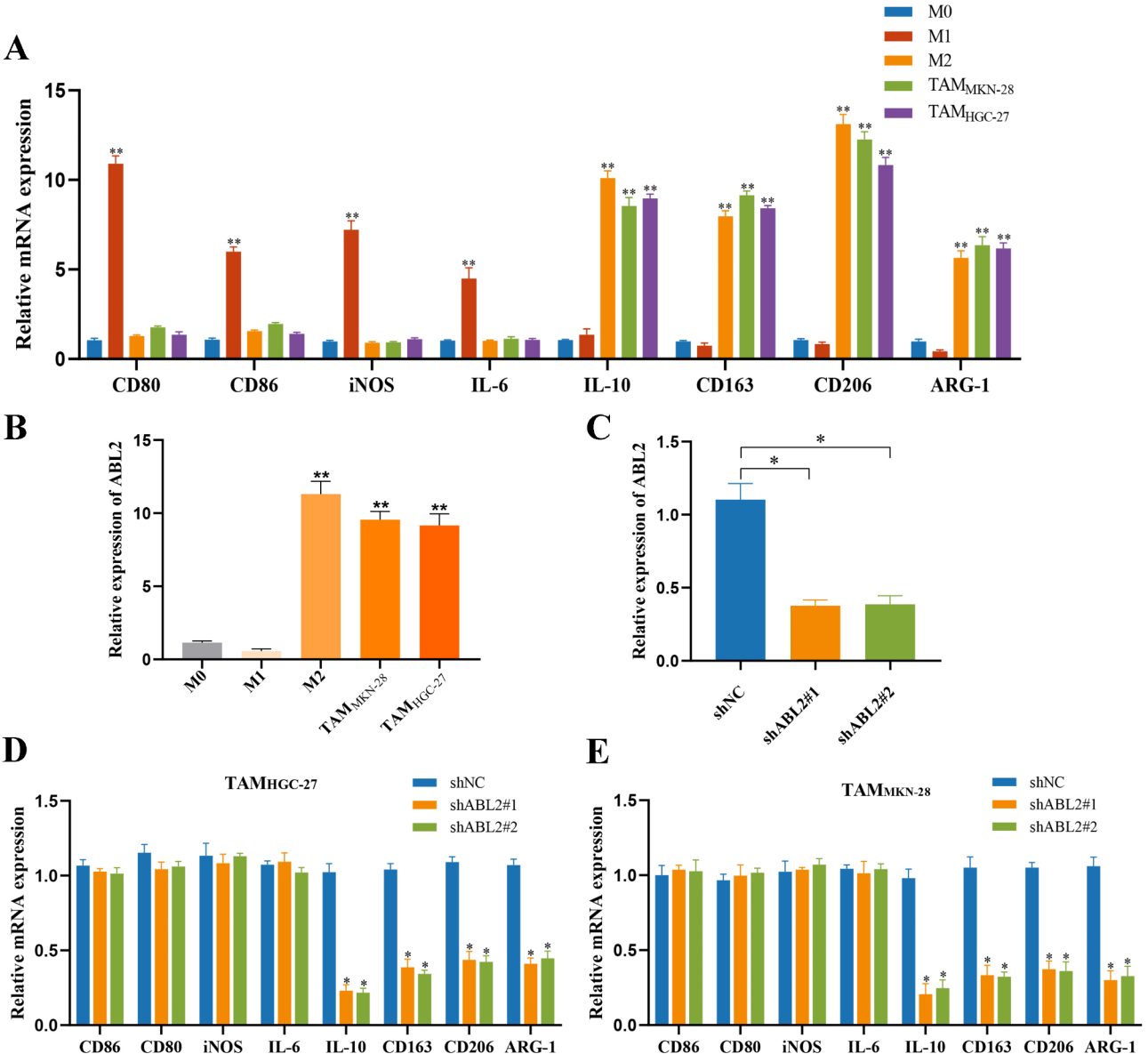

Fig. 9 The expression and function of ABL2 in Macrophages. **(A)** qRT-PCR assays were performed to identify the construction of M0, M1, M2, and TAMs. **(B)** The expression levels of ABL2 in M0, M1, M2, and TAMs. **(C)** The validation of ABL2 knockdown in TAMs. **(D and E)** qRT-PCR assays were performed to identify the effect of ABL2 on M2 macrophages polarization

lymphocytes, are major cellular components in the TME and play a pivotal role in regulating anti- and pro-tumor immune responses [37]. Recently, the functional interactions between protein kinases and macrophages have garnered significant attention in the field of immunology. For example, He et al. discovered that the activation patterns of multiple kinases were significantly different in M1 vs. M2 macrophage polarization through kinase-enrichment analysis of global quantitative proteomics and phosphoproteomics. Moreover, specific kinase inhibitors were found to selectively inhibit M2 macrophage polarization [38]. Dan et al. demonstrated that protein kinase RACK1 facilitated the polarization of M2 macrophage and inhibited the recruitment of macrophages, thereby leading to oral squamous cell carcinoma development [39]. Additionally, Wang et al. revealed that extracellular GP73 and protein kinase PKM2 synergistically induced M2-type macrophages polarization and angiogenesis, thus facilicating hepatocellular carcinoma progression [40]. In our studies, we further explored the role of the DE-KGsM in the microenvironment of GC. The results showed that the proportion of M2 macrophages exhibited both a significant correlation and a consistent trend with the DE-KGsM risk scores. Furthermore, TIDE is a computational algorithm that models two primary mechanisms of tumor immune

escape, namely T cell dysfunction and T cell exclusion. A High TIDE score represents a great potential of immune escape and poor response to immune checkpoint inhibitor (ICI) therapy. we found that high-DE-KGsM score patients had higher TIDE scores than GC patients with low-DE-KGsM scores. Therefore, we speculated that hub genes in the DE-KGsM might modulate the function of M2 macrophages in the TME, thereby influencing the progression and therapeutic efficacy of GC.

Based on scRNA-seq analysis, we found that the expression of ABL2 in the DE-KGsM was co-distributed with Macrophages in both GSE112302 and GSE167297 datasets. Therefore, ABL2 was identified as hub DE-KGs for further analysis. Then, ABL2 was found to be positively correlated with the tumor infiltration level of Macrophages M2 using MCPCOUNTER, CIBERSORT-ABS, TIMER, and QUANTISEQ algorithms. ssGSEA also indicated that immune-related functions, such as Type II IFN Reponse, Treg, and Macrophages were activated in the ABL2-high group. The proportion of TIICs, such as Macrophages M2, T cells CD8, and NK cells activated in the ABL2-high group was significantly higher than that in the ABL2-low group. We speculated that ABL2 might play an indispensable role in tumor immunity through regulating the polarization of M2 macrophages. In recent years, tumor-associated macrophages (TAMs), as the most abundant immune cells in TME, have attracted increasing attention from cancer researchers. TAMs refer to macrophages present in the TME or infiltrated into tumor tissues, primarily originating from circulating monocytes in peripheral blood [41, 42]. According to the differences in polarization state, secretion factors, and functions, TAMs can be divided into two subgroups: classically activated M1 macrophages and alternately activated M2 macrophages [43]. Most TAMs in the TME are M2 macrophages, which can promote angiogenesis, invasion, and metastasis of tumor cells [44–46]. ABL2, which belongs to the ABL tyrosine kinases, plays an essential role in modulating the proliferation, survival, and invasion of tumor cells [47]. Recently, enhanced ABL2 expression and activation have been detected in multiple tumors, including GC, lung cancer, and pancreatic ductal adenocarcinoma (PDAC), implicating a correlation between ABL2 activity and tumor progression [29, 48, 49]. For example, Liu et al. reported that high expression of ABL2 inhibits apoptosis of GC cells via caspase and Bcl2 family [29]. Hoj et al. revealed that ABL2 can regulate TAZ tyrosine phosphorylation and nuclear localization to facilitate lung adenocarcinoma brain metastasis [48]. Recently, Creeden et al. also identified increased ABL2 activity in PDAC cell lines and tissues using kinome arrays and bioinformatic pipelines [49]. Although the role of ABL2-mediated M2 macrophage polarization in GC has not been reported in previous studies, its significance should not be underestimated. According to the results of bioinformatics analyses, we also discovered that ABL2 was overexpressed in GC and related to the poor survival. We further conducted in vitro experiments to demonstrate the results of bioinformatics analysis. Based on the results of in vitro experiments, we found that the expression level of ABL2 was highly expressed in GC cells, TAMs, and M2 macrophages. Functional studies revealed that highly expressed ABL2 accelerated the proliferation, migration, and invasion of GC cells, as well as the polarization of M2 macrophages. Our findings suggested that ABL2 could serve as an immunological biomarker that modulates the polarization of M2 macrophages to facilitate the progression of GC. However, the detailed mechanisms underlying these findings still require further investigation.

Conclusion

In conclusion, we identified two molecular subtypes of GC patients according to 64 DE-KGs expression, which exhibited significant differences in the OS and the characteristics of the TME and TIICs. Using 101 combinations of 10 machine-learning algorithms, we established the optimal DE-KGsM, which could be a prognostic indicator in GC and associated with TIICs. More importantly, we found that the hub gene (ABL2) in the DE-KGsM might play an indispensable role in tumor immunity by regulating the status of macrophages. In vitro experiments further demonstrated that highly expressed ABL2 promoted the proliferation, migration, and invasion of GC cells, as well as the polarization of M2 macrophages. Our findings suggested that the DE-KGsM could be a powerful predictor of GC patients' survival and could be used to develop personalized therapy. Furthermore, ABL2 could be an immunological biomarker that modulates the polarization of M2 macrophages and took part in the progression of GC.

Supplementary Information

The online version contains supplementary material available at https://doi.org/10.1186/s13062-025-00636-9.

Supplementary Material 1

Supplementary Material 2

Acknowledgements

The authors gratefully acknowledge the TCGA and GEO databases for the availability of data.

Author contributions

Di Chen, and Zhifan Xiong designed the study, analyzed the data, and wrote the manuscript. Di Chen, Ju Huang, and Aiming Yang edited and revised the manuscript, generated figures and tables. All authors read and approved the final manuscript.

Funding
This study was supported by the Shandong Province Medical Health Science and Technology Project (202303031433) and Youth Research Start-up Fund, Yantai Yuhuangding Hospital, Qingdao University (202303).

Data availability
No datasets were generated or analysed during the current study.

Declarations

Ethics approval and consent to participate
In accordance with the Declaration of Helsinki, this study was approved by the Ethics Committee of Yantai Yuhuangding Hospital, Qingdao University.

Consent for publication
This study has not been published before, and all authors approved this publication.

Competing interests
The authors declare no competing interests.

Author details
[1]Department of Gastroenterology, Yantai Yuhuangding Hospital, Qingdao University, Yantai, China
[2]Department of Gastroenterology, Peking Union Medical College Hospital, Chinese Academy of Medical Sciences, Peking Union Medical College, Beijing 100730, China
[3]Department of Gastroenterology, Liyuan Hospital, Tongji Medical College, Huazhong University of Science and Technology, Wuhan 430077, China

Received: 26 December 2024 / Accepted: 16 March 2025
Published online: 24 March 2025

References

1. Sung H, Ferlay J, Siegel RL et al. Global Cancer Statistics 2020: GLOBOCAN Estimates of Incidence and Mortality Worldwide for 36 Cancers in 185 Countries. CA Cancer J Clin. 2021;71(3):209–249.https://doi.org/10.3322/caac.21660
2. Ji X, Bu ZD, Yan Y et al. The 8th edition of the American Joint Committee on Cancer tumor-node-metastasis staging system for gastric cancer is superior to the 7th edition: results from a Chinese mono-institutional study of 1663 patients. Gastric Cancer. 2018;21(4):643–652.https://doi.org/10.1007/s10120-017-0779-5
3. Pansy K, Uhl B, Krstic J et al. Immune Regulatory Processes of the Tumor Microenvironment under Malignant Conditions. Int J Mol Sci. 2021;22(24)https://doi.org/10.3390/ijms222413311
4. Zhang P, Feng J, Rui M et al. Integrating machine learning and single-cell analysis to uncover lung adenocarcinoma progression and prognostic biomarkers. J Cell Mol Med. 2024;28(13):e18516.https://doi.org/10.1111/jcmm.18516
5. Fu Y, Tao J, Liu T et al. Unbiasedly decoding the tumor microenvironment with single-cell multiomics analysis in pancreatic cancer. Mol Cancer. 2024;23(1):140.https://doi.org/10.1186/s12943-024-02050-7
6. Zhang P, Yang Z, Liu Z et al. Deciphering lung adenocarcinoma evolution: Integrative single-cell genomics identifies the prognostic lung progression associated signature. J Cell Mol Med. 2024;28(11):e18408.https://doi.org/10.1111/jcmm.18408
7. Zhang L, Cui Y, Mei J et al. Exploring cellular diversity in lung adenocarcinoma epithelium: Advancing prognostic methods and immunotherapeutic strategies. Cell Prolif. 2024;57(11):e13703.https://doi.org/10.1111/cpr.13703
8. Yasuda T, Wang YA. Gastric cancer immunosuppressive microenvironment heterogeneity: implications for therapy development. Trends Cancer. 2024;10(7):627–642.https://doi.org/10.1016/j.trecan.2024.03.008
9. Tiwari A, Trivedi R, Lin SY. Tumor microenvironment: barrier or opportunity towards effective cancer therapy. J Biomed Sci. 2022;29(1):83.https://doi.org/10.1186/s12929-022-00866-3
10. Bejarano L, Jordao MJC, Joyce JA. Therapeutic Targeting of the Tumor Microenvironment. Cancer Discov. 2021;11(4):933–959https://doi.org/10.1158/2159-8290.CD-20-1808
11. Zhang Y, Zhang Z. The history and advances in cancer immunotherapy: understanding the characteristics of tumor-infiltrating immune cells and their therapeutic implications. Cell Mol Immunol. 2020;17(8):807–821.https://doi.org/10.1038/s41423-020-0488-6
12. Feng J, Zhang P, Wang D et al. New strategies for lung cancer diagnosis and treatment: applications and advances in nanotechnology. Biomark Res. 2024;12(1):136.https://doi.org/10.1186/s40364-024-00686-7
13. Pan C, Liu H, Robins E et al. Next-generation immuno-oncology agents: current momentum shifts in cancer immunotherapy. J Hematol Oncol. 2020;13(1):29.https://doi.org/10.1186/s13045-020-00862-w
14. van den Bulk J, Verdegaal EM, de Miranda NF. Cancer immunotherapy: broadening the scope of targetable tumours. Open Biol. 2018;8(6).https://doi.org/10.1098/rsob.180037
15. Zhang L, Cui Y, Zhou G et al. Leveraging mitochondrial-programmed cell death dynamics to enhance prognostic accuracy and immunotherapy efficacy in lung adenocarcinoma. J Immunother Cancer. 2024;12(10)https://doi.org/10.1136/jitc-2024-010008
16. Chen LT, Satoh T, Ryu MH et al. A phase 3 study of nivolumab in previously treated advanced gastric or gastroesophageal junction cancer (ATTRACTION-2): 2-year update data. Gastric Cancer. 2020;23(3):510–519.https://doi.org/10.1007/s10120-019-01034-7
17. Jiang H, Zheng Y, Qian J et al. Safety and efficacy of sintilimab combined with oxaliplatin/capecitabine as first-line treatment in patients with locally advanced or metastatic gastric/gastroesophageal junction adenocarcinoma in a phase Ib clinical trial. BMC Cancer. 2020;20(1):760.https://doi.org/10.1186/s12885-020-07251-z
18. Kornev AP, Taylor SS. Dynamics-Driven Allostery in Protein Kinases. Trends Biochem Sci. 2015;40(11):628–647https://doi.org/10.1016/j.tibs.2015.09.002
19. Manning G, Whyte DB, Martinez R et al. The protein kinase complement of the human genome. Science. 2002;298(5600):1912–1934.https://doi.org/10.1126/science.1075762
20. Lu Z, Hunter T. Degradation of activated protein kinases by ubiquitination. Annu Rev Biochem. 2009;78:435–475https://doi.org/10.1146/annurev.biochem.013008.092711
21. Cohen P, Cross D, Janne PA. Kinase drug discovery 20 years after imatinib: progress and future directions. Nat Rev Drug Discov. 2021;20(7):551–569.https://doi.org/10.1038/s41573-021-00195-4
22. Blume-Jensen P, Hunter T. Oncogenic kinase signalling. Nature. 2001;411(6835):355–365.https://doi.org/10.1038/35077225
23. Huang G, Shi LZ, Chi H. Regulation of JNK and p38 MAPK in the immune system: signal integration, propagation and termination. Cytokine. 2009;48(3):161–169.https://doi.org/10.1016/j.cyto.2009.08.002
24. Tam SY, Law HK. JNK in Tumor Microenvironment: Present Findings and Challenges in Clinical Translation. Cancers (Basel). 2021;13(9).https://doi.org/10.3390/cancers13092196
25. Ebelt ND, Cantrell MA, Van Den Berg CL. c-Jun N-Terminal Kinases Mediate a Wide Range of Targets in the Metastatic Cascade. Genes Cancer. 2013;4(9–10):378–387.https://doi.org/10.1177/1947601913485413
26. Hoj JP, Mayro B, Pendergast AM. The ABL2 kinase regulates an HSF1-dependent transcriptional program required for lung adenocarcinoma brain metastasis. Proc Natl Acad Sci U S A. 2020;117(52):33486–33495.https://doi.org/10.1073/pnas.2007991117
27. Liu Y, Cao J, Zhu YN et al. C1222C Deletion in Exon 8 of ABL1 Is Involved in Carcinogenesis and Cell Cycle Control of Colorectal Cancer Through IRS1/PI3K/Akt Pathway. Front Oncol. 2020. https://doi.org/10.3389/fonc.2020.01385
28. Wang W, Li M, Ponnusamy S et al. ABL1-dependent OTULIN phosphorylation promotes genotoxic Wnt/beta-catenin activation to enhance drug resistance in breast cancers. Nat Commun. 2020;11(1):3965.https://doi.org/10.1038/s41467-020-17770-9
29. Liu Y, Shao C, Zhu L et al. High Expression of ABL2 Suppresses Apoptosis in Gastric Cancer. Dig Dis Sci. 2018;63(9):2294–2300.https://doi.org/10.1007/s10620-018-5111-7
30. Greuber EK, Smith-Pearson P, Wang J et al. Role of ABL family kinases in cancer: from leukaemia to solid tumours. Nat Rev Cancer. 2013;13(8):559–571.https://doi.org/10.1038/nrc3563
31. Afrose SS, Junaid M, Akter Y et al. Targeting kinases with thymoquinone: a molecular approach to cancer therapeutics. Drug Discov Today. 2020;25(12):2294–2306.https://doi.org/10.1016/j.drudis.2020.07.019

32. Fleuren ED, Zhang L, Wu J et al. The kinome 'at large' in cancer. Nat Rev Cancer. 2016;16(2):83–98.https://doi.org/10.1038/nrc.2015.18
33. Elmas A, Tharakan S, Jaladanki S et al. Pan-cancer proteogenomic investigations identify post-transcriptional kinase targets. Commun Biol. 2021;4(1):1112.https://doi.org/10.1038/s42003-021-02636-7
34. Guo Z, Zhou C, Zhou L et al. Overexpression of DAPK1-mediated inhibition of IKKbeta/CSN5/PD-L1 axis enhances natural killer cell killing ability and inhibits tumor immune evasion in gastric cancer. Cell Immunol. 2022;372:104469.https://doi.org/10.1016/j.cellimm.2021.104469
35. Hsu HP, Wang CY, Hsieh PY et al. Knockdown of serine/threonine-protein kinase 24 promotes tumorigenesis and myeloid-derived suppressor cell expansion in an orthotopic immunocompetent gastric cancer animal model. J Cancer. 2020;11(1):213–228.https://doi.org/10.7150/jca.35821
36. Wu X, Qu D, Weygant N et al. Cancer Stem Cell Marker DCLK1 Correlates with Tumorigenic Immune Infiltrates in the Colon and Gastric Adenocarcinoma Microenvironments. Cancers (Basel). 2020;12(2)https://doi.org/10.3390/cancers12020274
37. Lei X, Lei Y, Li JK et al. Immune cells within the tumor microenvironment: Biological functions and roles in cancer immunotherapy. Cancer Lett. 2020;470:126–133.https://doi.org/10.1016/j.canlet.2019.11.009
38. He L, Jhong JH, Chen Q et al. Global characterization of macrophage polarization mechanisms and identification of M2-type polarization inhibitors. Cell Rep. 2021;37(5):109955.https://doi.org/10.1016/j.celrep.2021.109955
39. Dan H, Liu S, Liu J et al. RACK1 promotes cancer progression by increasing the M2/M1 macrophage ratio via the NF-kappaB pathway in oral squamous cell carcinoma. Mol Oncol. 2020;14(4):795–807.https://doi.org/10.1002/1878-0261.12644
40. Wang S, Zhang T, Zhou Y et al. GP73-mediated secretion of PKM2 and GP73 promotes angiogenesis and M2-like macrophage polarization in hepatocellular carcinoma. Cell Death Dis. 2025;16(1):69.https://doi.org/10.1038/s41419-025-07391-9
41. Liang Y, Liu Y, Zhang Q et al. Tumor-derived extracellular vesicles containing microRNA-1290 promote immune escape of cancer cells through the Grhl2/ZEB1/PD-L1 axis in gastric cancer. Transl Res. 2021;231:102–112.https://doi.org/10.1016/j.trsl.2020.12.003
42. Yoon CJ, Chang MS, Kim DH et al. Epstein-Barr virus-encoded miR-BART5-5p upregulates PD-L1 through PIAS3/pSTAT3 modulation, worsening clinical outcomes of PD-L1-positive gastric carcinomas. Gastric Cancer. 2020;23(5):780–795.https://doi.org/10.1007/s10120-020-01059-3
43. Wang CJ, Zhu CC, Xu J et al. The lncRNA UCA1 promotes proliferation, migration, immune escape and inhibits apoptosis in gastric cancer by sponging anti-tumor miRNAs. Mol Cancer. 2019;18(1):115.https://doi.org/10.1186/s12943-019-1032-0
44. Ding L, Li Q, Chakrabarti J et al. MiR130b from Schlafen4(+) MDSCs stimulates epithelial proliferation and correlates with preneoplastic changes prior to gastric cancer. Gut. 2020;69(10):1750–1761.https://doi.org/10.1136/gutjnl-2019-318817
45. Ren W, Zhang X, Li W et al. Exosomal miRNA-107 induces myeloid-derived suppressor cell expansion in gastric cancer. Cancer Manag Res. 2019;11:4023–4040.https://doi.org/10.2147/CMAR.S198886
46. Xiong G, Yang L, Chen Y et al. Linc-POU3F3 promotes cell proliferation in gastric cancer via increasing T-reg distribution. Am J Transl Res. 2015;7(11):2262–2269.
47. Luttman JH, Colemon A, Mayro B et al. Role of the ABL tyrosine kinases in the epithelial-mesenchymal transition and the metastatic cascade. Cell Commun Signal. 2021;19(1):59.https://doi.org/10.1186/s12964-021-00739-6
48. Hoj JP, Mayro B, Pendergast AM. A TAZ-AXL-ABL2 Feed-Forward Signaling Axis Promotes Lung Adenocarcinoma Brain Metastasis. Cell Rep. 2019;29(11):3421–3434 https://doi.org/10.1016/j.celrep.2019.11.018
49. Creeden JF, Alganem K, Imami AS et al. Kinome Array Profiling of Patient-Derived Pancreatic Ductal Adenocarcinoma Identifies Differentially Active Protein Tyrosine Kinases. Int J Mol Sci. 2020;21(22)https://doi.org/10.3390/ijms21228679

Publisher's note